Histol Histopathol (2020) 35: 1115-1123

http://www.hh.um.es

Histology and Histopathology
From Cell Biology to Tissue Engineering

Nuclei detection in hepatocellular carcinoma and dysplastic liver nodules in histopathology images using bootstrap regression

Lekshmi Kalinathan[1], Ruba Soundar Kathavarayan[2], Madheswari Kanmani[1] and Nagendram Dinakaran[3]

[1]SSN College of Engineering, Anna University, Chennai, [2]PSR Engineering College, Anna University, Sivakasi and [3]Gastroenterologist, Meenakshi Medical College and Research Institute, Maher University, Kanchipuram, India

Summary. Hepatocellular carcinoma (HCC) is the most common primary malignant neoplasm of the liver representing the fifth most common malignancy worldwide. This tumor is more common in men than women, with a ratio of 2.7:1. Unlike HCC, Dysplasia is the precancerous nature of liver nodules and is characterized by cellular and nuclear enlargement, nuclear pleomorphism, and multinucleation. Area based Adaptive Expectation Maximization (EM) uses texture, layout, and context features of cells, and grows clusters to obtain texton maps of nucleus. A discriminative model of nucleus and cytoplastic changes of tumor is built by incorporating texture, layout, and context information efficiently. A bootsrap regression model of nuclei and cytoplastic changes are built by incorporating the aforementioned features efficiently. Mean squared error, Peak Signal to Noise ratio and Dice similarity values are used to evaluate the method's classification performance. The proposed method provides high classification and segmentation accuracy of nucleus and extra nuclear content in HCC and dysplasia, which are exceedingly textured in histopathology images, when compared to Adaptive K means, EM method and the state-of-the-art method, Convolutional Neural Networks (CNN). As texton detection reduces the cluttered background of nuclei, the proposed method would be a convenient mechanism for the classification of nuclei and non-nuclear features. In conclusion, this system can detect more eligible cells of precancerous nature as well as malignant cells even in a cluttered background of nuclei.

Key words: Histopatholgy, Dysplasia, Hepatocellular Carcinoma, Hepatic tumor, Classification

Offprint requests to: Lekshmi Kalinathan, Associate Professor, Department of Computer Science and Engineering, SSN College of Engg, Anna University, Chennai, India. e-mail: lekshmik@ssn.edu.in
DOI: 10.14670/HH-18-240

Introduction

Hepatic Nodular lesions are predominantly composed of either hepatocytes or neoplastic cells with hepatocytic features. In dysplasia, cells with dysplastic features often form groups, which were termed "dysplastic foci" by the IWP. Dysplastic nodules are nodular lesions with cytologic and structural atypia, indicative of precancerous change (Wanless, 1995; Andrea et al., 2016). The groups of crowded, small, atypical hepatocytes of dysplastic foci were termed "Small cell change" of hepatocytes by the IWP (Hytiroglou et al., 2007).

Molecular studies have provided the precancerous nature of small cell change (Marchio et al., 2001; Plentz et al., 2007; American Cancer Society, 2018). However, the small sized hepatocytes are often seen in cirrhotic livers, as a result of regeneration (Nakanuma and Hirata, 1993; American Cancer Society, 2018). Therefore, small cell size alone is not sufficient evidence of precancerous

change in the absence of cytologic atypia. This cytological change was originally described as "liver cell dysplasia" (Anthony et al., 1973; Stewart and Wild, 2014). These dysplastic lesions evolve into Hepatocellular carcinoma over time (Takayama et al., 1990; Sakamoto and Hirohashi, 1998). Therfore, focal HCC may occasionally be found on microscopic examination of dysplastic nodules (Arakawa et al., 1986).

Images of IR spectra were recorded (Perkin Elmer Spotlight 300) using FTIR microscope. Instead of evaluating more than 192 million measured transmittances, the original spectrum of 1626 points at each image pixel were reduced to 64 values at each pixel using IR metrics (Fernandez at al., 2005). Using K-means cluster analysis, 64 IR spectral points are distinguished into 5 groups based on six IR metrics (Zhaomin et al., 2013). The centroid for each pixel in image was calculated per group based on similarity (or a "distance") between a particular image pixel and the average metric scores of the group. According to the minimization of sum of "distances" for each group, membership of image pixels in each group changes. Finally, each image pixel with similar metrics is organised into a group.

This paper investigates the problems of achieving automatic detection, recognition, and segmentation of nuclei in HCC and Dysplasia in histopathology images. The proposed system should automatically partition the given histopath image into meaningful regions, where the required regions can be labeled with a specific object class color. The treatment of liver tumor in early stage can cure it in certain cases, yet the long term anticipation essentially relies on upon the vicinity and severity of liver damage and its extension (Andrea et al., 2016).

A hybrid diagnosis method is proposed to detect the nucleus and non-features of HCC and dysplasia automatically by utilizing histopathology images of cryostat sections. This paper is organized as follows. Immediately below, we discuss related work. Various clustering, segmentation methods and the proposed method, which uses Conditional Random Field (CRF) to generate a model for nucleus and other non-features, are discussed in Section 2. In the aforementioned Section 2, the discussion of system design consists of texture-layout filters and their combination leads to segregation of nucleus from non-features. Finally, the proposed method is evaluated and compared with existing related work. The performance of the proposed method is discussed and concluded in Section 3.

Materials and methods

As this work is a review examination, the images utilized as a part of this examination work are the records of already analyzed patients. We acquired four normal, four dysplasia and five hepatocellular carcinoma images from Global Hospital, Chennai with the magnification factors of 10x, 200x and 400x sizes respectively. The training dataset comprises two normal, two dysplasia and three HCC images which roughly incorporates 4900 nuclei and cytoplasmic cells. Also, the testing set is comprised of the other two normal, two dysplasia and two HCC images which include about 4200 nuclei and cytoplasm cells. The study is endorsed by Institutional Ethics Committee and all sample images had been stored in RGB color space in a Joint Photographic Experts Group (JPEG) format where the size of each image was 1600×1200 pixels.

Various approaches of segmentation

The regions found by bottom-up segmentation are labelled with textual class labels of images, trained in a

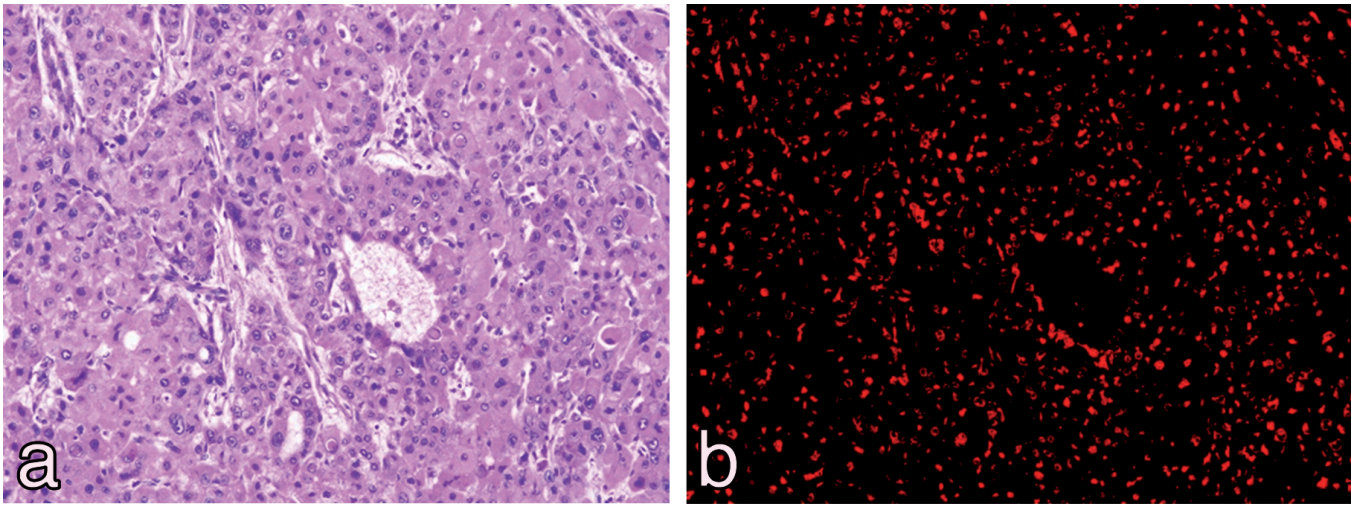

Fig. 1. Example results of new simultaneous tumor nucleus recognition and segmentation algorithm.

classifier (Duygulu et al., 2002). However, semantic objects are not correlated with such segmentations and hence in the proposed system, segmentation and recognition of nuclei are performed in the same unified framework rather than in two separate steps. At a high computational cost, such a unified approach was presented in the study (Zhuowen at al., 2005). However, in images labeled using a unary classifier, spatially coherent segmentations are not achieved (Konishi and Yuille, 2000). In K-means clustering, it is not easy to clearly identify initial K seeds of textual class labels of nucleus and non-nuclei in the images (Rohit and Gaikwad, 2013). Adaptive K-means algorithm partitions the given dataset without the initial identification of seeds to represent clusters (Bhagwati and Sinha, 2010). Also this algorithm faces the problem of getting more local optima, EM algorithm finds the solution for the same (Tsai et al., 2001). EM algorithm assigns data points partially to different clusters using a probabilistic distribution, where each data point belongs to the cluster with the highest probability (Moon et al., 2002). The molecular analyses require the investigation of somatic genetic alterations, gene or protein expression, or even circulating tumour markers. However, histopathological classification remains the gold standard for diagnosis in most instances (Nagtegaal et al., 2019). The proposed method grows clusters with the textons of images without having the initial selection of clusters and also stops the generation of clusters based on area function automatically, and trained in the classifier, which generates a descriminative model with bootstrap regression coefficients to improve the classification accuracy of nuclei from other components as shown in Fig. 1a,b. Representation of a pixel in higher dimensions always leads to high computational cost in the state-of-art method (Shelhamer et al., 2017). However, the existing methods and convolutional networks work on the color images whose objects to be segmented are highly textured and highly structured.

A conditional random field model of classes

Conditional distribution over the class labeling is learned using a Conditional random field (CRF) model (Lafferty et al., 2001; Shotton et al., 2006; Kuang et al., 2012), for a given image. Texture layout, color, location, and edge cues are incorporated into a single unified model. Conditional probability of the class labels c for a pixel to be either nucleus or non-nucleus is defined as

$$\log P(c \mid x,\theta) = \sum_i \overbrace{\psi_i\left(c_i,x_i;\theta_\psi\right)}^{texture\ layout} + \overbrace{\pi\left(c_i,x_i;\theta_\pi\right)}^{color} + \overbrace{\lambda\left(c_i,i;\theta_\lambda\right)}^{location} + \sum_{(i,j)\in\varepsilon} \overbrace{\phi\left(c_i,c_j,g_{ij}(x);\theta_\phi\right)}^{edge} - \log Z(\theta,x)$$

where ε is the set of edges, $\theta=(\theta_\psi,\theta_\gamma,\theta_\lambda,\theta_\phi)$ are the model parameters corresponding to texture-layout, color, location and edge respectively, i and j correspond to positions of pixels in the image, $g_{ij}(X)$ represents the

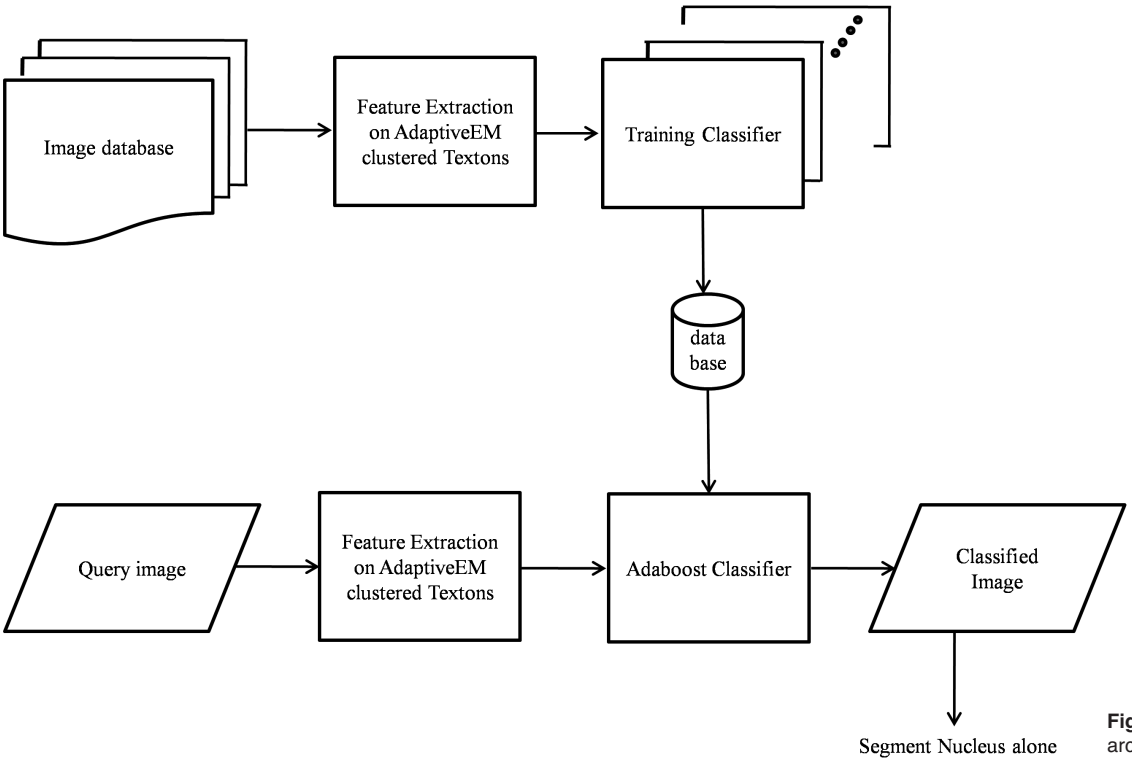

Fig. 2. Proposed system architecture.

edge feature and Z(θ, x) is the partition function which normalizes the distribution.

Proposed system

The overall system architecture is explained in (Fig. 2). The system design describes the phases of modules of the system under Textonization, building classifier model, testing and performance evaluation.

Textonization

Histopathology images are convolved with 17 dimensional convolution filter bank to obtain 17D responses. The filter operations can intensify or reduce certain image details and enable an easier or faster evaluation of the size of nucleus. 17-D Convolution filter banks are generated by applying Gaussians to all three HSV (Hue, Saturation and Value) channels, while the other filters are applied only to the luminance. When three Gaussian filters, are applied to HSV channels, 9D responses are obtained and four Laplacian of Gaussian filters (LoG) and the four first order Derivatives of Gaussians are applied to luminance produce 4D responses each; a total of 17D responses.

The 17D filter responses obtained are convolved with the training images, which are automatically clustered using Modified EM algorithm to generate a texton map. In order to calculate texture-layout filter responses in constant time, an integral image is built for

Algorithm for construction of Texton Map

Input: Feature responses of training images

Output: Texton Map

Step 1: Initialization of parameters φ, as k=1, μ_k, Σ_k, $p(c_k)$ and biggest_comp_0= -1

Step 2: Computation of parameters φ, using EM based on k clusters so far generated

Repeat until convergence {

(E-step) for each i, k, set

$$p(C_k|x_i) = w_k(x) = \frac{w_k \bullet f_k(x|\phi_k)}{\sum_i w_i \bullet f_i(x|\phi_k)}$$

(M-step) Update the parameters μk, Vk and p(Ck)

$$\mu_{k+1} = \frac{\sum_i w_k(x_i) \bullet x_i}{\sum_i w_k(x_i)}$$

$$V_{k+1} = \frac{\sum_i w_k(x_i) \bullet (x_i - \mu_k) \bullet (x_i - \mu_k)^\tau}{\sum_i w_k(x_i)}$$

$$p(C_{k+1}) = \frac{\sum_i p(c_k|xi)}{N}$$

}

Do generate the clusters using area based Adaptative EM

```
biggest= -1
for each Feature Response x_i and φ_k
        c= compute f_k(x_i/φ_k)
        n= count the no of connected components on c
        for each conn_compn
                area_comp= computearea(conn:compn)
                if area_comp>biggest
                        biggest= area_comp
        end for
        biggest_comp_k= biggest
end for
```

Step 3: Repeat step 2 **until** $\text{biggest\_comp}_k > \text{biggest\_comp}_{k-1}$ by incrementing k further

Fig. 3. Algorithm for construction of Texton map using area based AdaptiveEM.

each channel. Area based Adaptive EM method runs on these filter responses to generate clusters automatically, thus providing the texton map. To compute the texture-layout filter responses in constant time, an integral histogram is computed for each texton with one bin (Porikli, 2005).

$$f_{[i,r,t]} = \hat{T}^{(t)}_{rbr} - \hat{T}^{(t)}_{rbl} - \hat{T}^{(t)}_{rtr} + \hat{T}^{(t)}_{rtl}$$

Where rbr, rbl, rtr and rtl denote the bottom right, bottom left, top right and top left corners of rectangle r.

A hybrid diagnosis method is proposed to detect the aforementioned textons automatically in histopathology images. An area function adaptation scheme that uses the EM model grows the clusters without the need for initial selection of clusters. With the feature responses obtained, clusters are generated automatically. As no component in any cluster is bigger than the texton of nucleus, the algorithm stops generating the clusters after the generation of texton of nucleus, whose cluster number is k. Thus the n filter responses are partitioned into k clusters where each response serves as a prototype of a cluster, belongs to the nearest mean cluster. The finding of these studies (Lafferty et al., 2001; Bryan et al., 2008; Kuang et al., 2012) showed that parameters (μ_k mean, Σ_k var, $p(c_k)$ weights) are updated iteratively until they converge. With these updated parameters, clusters of textons are generated and the generation stops automatically when the area of the biggest component nucleus is found (Fig. 3).

Building Classifier Model

Automatic feature selection and learning of texture-layout potentials are carried out by boosting process (Freund and Schapire, 1999). A strong classifier H(ci) can be built by summing up 'weak classifiers' iteratively (Friedman et al., 2000). Using a thresholded feature response as a decision stump, weak classifiers can be found, in which the optimal parameter coefficients are estimated using bootstrap regression coefficients to improve the classification accuracy of nucleus of various tumors in histopathology images (Hiroshi and Masaaki, 2003). Bootstrap can provide more accurate inferences in small size nuclei and complex clustered samples of nuclei. A decision stump of each weak-learner is defined as

$$h(c_i) = \begin{cases} a\left\lfloor f_{[i,r,t]} > \theta \right\rfloor + b \\ k^c \end{cases} \quad if\ \mathrm{c} \in \mathrm{C}\ otherwise$$

Where

$$k^c = \frac{\sum_i w_i^c z_i^c}{\sum_i w_i^c}$$

k^c is the numbers of training features of each class when $c \notin C$. $f_{[i,r,t]}$ represents the corresponding feature response at position i.

$$a = \frac{\sum_{c \in N} \sum_{i=1}^{n} \left(f_{[i,r,t]} - \overline{f_{[i,r,t]}}\right)\left(z_i^c - \overline{z_i^c}\right)}{\sum_{i=1}^{n} \left(f_{[i,r,t]} - \overline{f_{[i,r,t]}}\right)^2}$$

$$b = \sum_{c \in N} \left(\sum_{i=1}^{n} \overline{z_i^c} - a\left(f_{[i,r,t]}\right) \right)$$

To enable a single feature of nucleus or non-features to classify several classes at once, a weak classifier is shared between a set of classes. For those classes that share the feature, weak learner gives hi(c) belonging to a + b, b depending on the comparison of feature. Round m chooses a new weak learner by minimizing an error function E incorporating the weights.

$$E = \sum_{c \in N} \sum_{i=1}^{n} w_i^c \left(z_i^c - a\left(f_{i,r,t} > \theta\right) + b\right)^2$$

A strong classifier is built by summing the classification confidence of M weak learners.

$$H(c_i) = \sum_{m-1}^{M} h_m(c_i)$$

Testing image

The test image is textonized and extracts features (nuclei) and non-features from it. These features are tested with Adaboost algorithm to obtain an image, classified as two classes of nucleus (red) and non-features (black) (Fig. 4). The sample images are tested and their segmented outputs are shown in Fig. 5.

Results

This work is mostly focused on segmenting the nucleus and the extracellular nuclei changes of the various tumors irrespective of their sizes. This implementation should have the ability to obtain histopathology images from patients. This implementation is carried out in matlab. The texton feature responses are trained in AdaBoost classifier for 100 rounds to build the discriminative model to gain more accuracy using bootsrap regression coefficients discussed in Table 1. The knowledge about the nuclei provided by the expert pathologist from the Global Hospital is used to verify the accuracy of the segmented nuclei against the groundtruths. The diagnostication accuracy of the method is very high when compared to the conventional methods like Adaptive k-means and EM, and state of art method, CNN. Also, the segmented nuclei with this method provides a better understanding in infected nuclei with respect to size of the same in a malignant cell.

Performance evaluation

Three metric is followed here by MSE, PSNR and DSC. MSE is close to zero relative to the magnitude of at least one of the estimated treatment effects. It represents the mean squared error rate between 0 to 1. The lower the value of MSE, the lower the error. From the segmentation techniques, the error rate of the proposed method is 0.01. The higher the PSNR, the better the quality of image. Typical values for an image are between 30dB and 50dB, when the PSNR is greater than dB. Dice Similarity metric is always between 0 and 1 with higher values returning a better match between automatic and manual segmentation (Casciaro et al., 2012).

$$MSE = \frac{1}{n}\left(\sum_{i=1}^{C}(t_i - n_{ii})^2\right)$$

$$\text{where } t_i = \sum_{j=1}^{z} n_{ij} \qquad n = \sum_{i=1}^{C} t_i$$

being the total number of pixels in an image.

$$PSNR = 10 \times \log_{10}\left(\frac{255 \times 255}{(MSE)}\right)$$

$$DSC = \frac{2\left(\sum_{i=1}^{C}(t_i \cap n_{ii})\right)}{2\sum_{i=1}^{C} t_i + \sum_{i=1}^{C} n_{ii}}$$

$$Accuracy = \sum_{i=1}^{C} \frac{n_{ii}}{t_i}$$

It is clear that to segment the nuclei of hepatic tumors like HCC and dysplasia, the proposed method results in a much higher efficiency than any of the algorithms in this field (Table 1).

Discussion

It is incredibly important for a patient to segment the multi-nucleated liver tumors in histology images. The segmentation of nuclei in HCC and dysplastic nodules is carried out and analyzed with histological images. Automatic segmentation techniques of identifying nuclei in HCC and dysplasia from histological images have been here implemented and the results are shown in Table 1. Boosting classifier gradually selects new texture-layout filters to improve classification accuracy. As texture layout filters are added, the classification accuracy improves greatly and after 100 rounds, a very accurate classification is given. Furthermore, the accuracy of classification with respect to the validation set results in 89.51% for nuceli of HCC and dysplasia, in which accuracy is measured as the pixelwise segmentation accuracy. Our proposed method assists greatly to detect all nuclei irrespective of their sizes efficiently, and provides a better recall than EM without compromising the computational cost and accuracy unlike the convolutional networks and the aforementioned conventional methods.

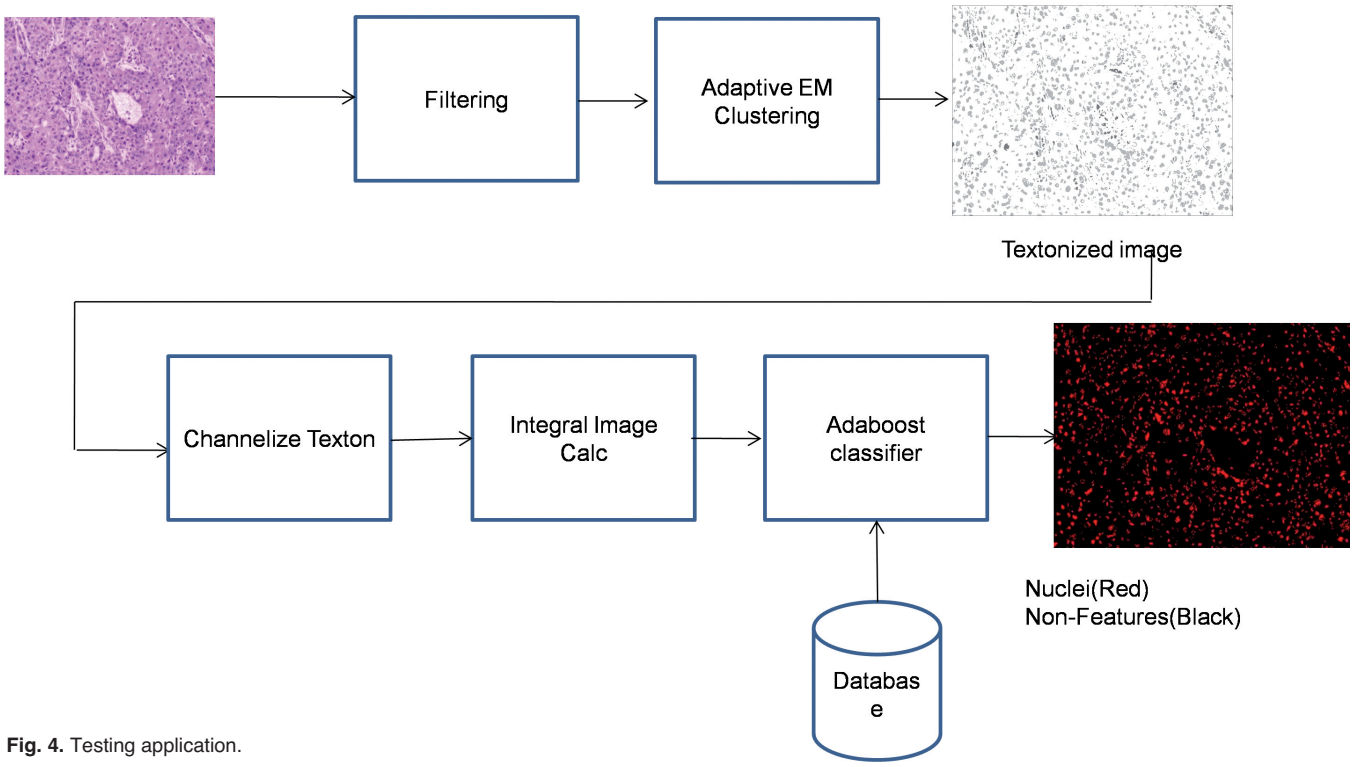

Fig. 4. Testing application.

Conclusion

From the analyses of the performance metrics calculated for the various automatic diagnosticating techniques, it is observed that the algorithm results in a much higher efficiency than any of the existing algorithms, with respect to the nucleus and extra cellular nucleus changes of the respective tumors. This system is

Table 1. Quantitative comparison of existing approaches with the proposed system.

Segmentation Techniques	MSE1	PSNR2	DSC3	Sensitivity	Specificity	FPR4	Accuracy %
Proposed	0.01	73.36	0.55	0.99	0.23	0.77	89.51
Adaptive-K-Means	0.13	58.76	0.33	0.86	0.12	0.88	52.11
EM5	0.05	63.04	0.29	0.86	0.16	0.84	56.95
Convolutional Networks	0.08	59.92	0.54	0.92	0.01	0.99	69.26

1, Mean Squared Error; 2, Peak signal-to-noise ratio; 3, Dice Similarity Coefficient; 4, False Positive Rate; 5, Expectation Maximization.

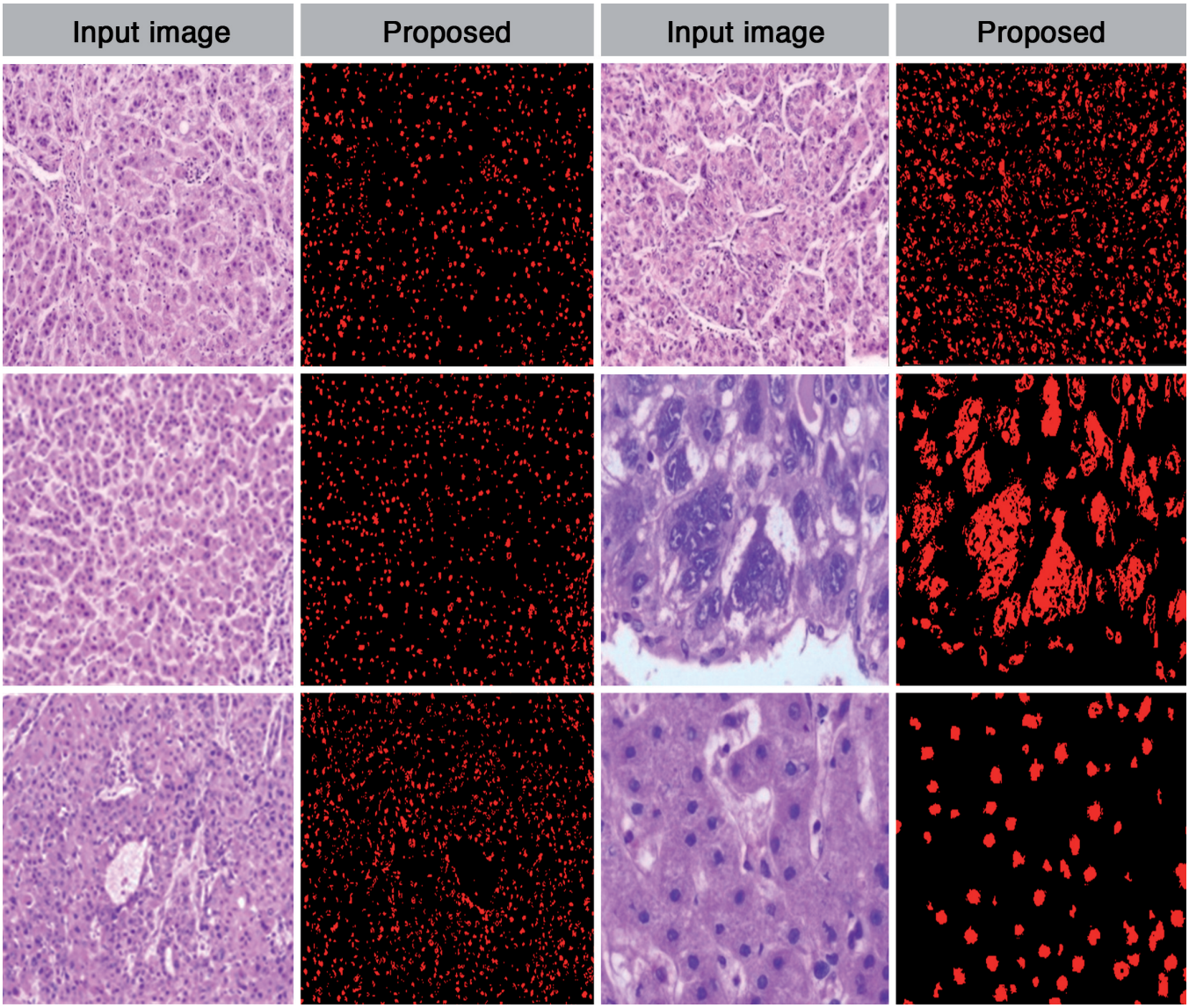

Fig. 5. Visual demonstration of nuclei detection.

low cost, non-invasive and can detect cells of precancerous nature as well as malignant cells even in cluttered backgrounds of nuclei with much higher efficiency. However, it does not provide the etiology. In the future, more histopathology images of infected cells need to be collected and algorithm analyses performed to diagnose cytoplastic changes along with the use of stromal and cellular nuclei changes.

Acknowledgements. This work was supported by the Gleneagles Global Hospital and Health City, Chennai under Grant HR/2016/MS/009. We want to thank and deep sense of gratitude to Dr. K.S. Mouleeswaran, Pathologist of Gleneagles Global Hospital for providing the medical image data and interpretation for the analysis. Also, we would like to thank Prof. C. Emmanuel, Director-Academics and Research in the Global Hospitals and Health City, Chennai, for his kind collaboration in this study. Dr. K.S. Mouleeswaran has verified our experimental studies in the segmentation of nucleus and helped us a lot in getting a better insight and assessing the extent and number of liver metastases in histopathology images.

References

American Cancer Society. (2018). Cancer Facts & Figures 2018. Atlanta. American Cancer Society.

Andrea M., Ramy Ibrahim K.J. and Elisabetta B. (2016). Progression and natural history of nonalcoholic fatty liver disease in adults. Clin. Liver Dis. 20, 313-324.

Anthony P.P., Vogel C.L. and Barker L.E. (1973). Liver cell dysplasia: a premalignant condition. J. Clin. Pathol. 26, 217-223.

Arakawa M., Kage M., Sugihara S., Nakashima T., Suenaga M. and Okuda K. (1986). Emergence of malignant lesions within an adenomatous hyperplastic nodule in a cirrhotic liver. Observations in five cases. Gastroenterology 91, 198-208.

Bhagwati C.P and Sinha G.R. (2010). an Adaptive K-means clustering algorithm for breast image segmentation. Int. J. Comput. Applicat. 10, 35-38.

Bryan C.R., Antonio T., Kevin P.M. and William T.F. (2008). LabelMe: A database and webbased tool for image annotation. Int. J. Comput. Vis. 77, 157-173.

Casciaro S. Franchini R. Massoptier L. Casciaro E. Conversano F. Malvasi A. and Lay-Ekuakille A. (2012). Fully automatic segmentations of liver and hepatic tumors from 3-D computed tomography abdominal images: comparative evaluation of two automatic methods. IEEE Sensors J. 12, 464-473.

Duygulu K., Barnard, J.F.G., de Freitas and Forsyth D.A. (2002). Object recognition as machine translation: Learning a lexicon for a fixed image vocabulary. Proc. Eur. Conf. Comput. Vis. Springer-Verlag Berlin Heidelberg. 2353, 97-112.

Fernandez D.C., Bhargava R, Hewitt S.M and Levin I.W. (2005). Infrared spectroscopic imaging for histopathologic recognition. Nat. Biotech. 23, 469-474.

Freund Y. and Schapire R.E. (1999). A short introduction to boosting. J. Jpn. Soc. Artific. Intellig. 14, 771-780.

Friedman J., Hastie T. and Tibshirani R. (2000). Additive logistic regression: a statistical view of boosting. Ann. Statistics. 28, 337-407.

Hiroshi K. and Masaaki H. (2003). Statistics Calculator - a new method of probability calculation. Statistics Front. Sci. 11, 41-59.

Hytiroglou P. (2004). Morphological changes of early human hepatocarcinogenesis. Semin. Liver Dis. 24, 65-75.

Hytiroglou P., Park, Y.N., Krinsky G. and Theise N.D. (2007). Hepatic precancerous lesions and small hepatocellular carcinoma, Gastroenterol. Clin. N. Am. 36, 867-887.

Konishi S. and Yuille A.L. (2000). Statistical cues for domain specific image segmentation with performance analysis. Proc. IEEE Conf. Comput. Vis. Pattern Recognit. 1, 125-132.

Kuang Z., Schnieders D., Zhou H., Wong K.K., Yu Y. and Peng B. (2012). Learning image-specific parameters for interactive segmentation. IEEE Conf. Comput. Vis. Pattern Recognit. 590-597.

Lafferty J., McCallum A. and Pereira F. (2001). Conditional random fields: probabilistic models for segmenting and labeling sequence data. Proc. Int. Conf. Machine Learning 282-289.

Marchio A., Terris B., Meddeb M., Pineau P., Duverger A., Tiollais P., Bernhei A. and Dejean A. (2001). Chromosomal abnormalities in liver cell dysplasia detected by comparative genome hybridisation. Mol. Pathol. 54, 270-274.

Moon N., Bullitt E., Leemput K.V. and Gerig G. (2002). Model-Based brain and tumor segmentation. IEEE 1, 528-531.

Nagtegaal I.D., Odze R.D., Klimstra D., Paradis V., Rugge M., Schirmacher P., Washington M.K., Carneiro F. and Cree I.A. (2019). The 2019 WHO classification of tumours of the digestive system. Histopathology 76, 182-188.

Nakanuma Y. and Hirata K. (1993). Unusual hepatocellular lesions in primary biliary cirrhosis resembling but unrelated to hepatocellular carcinoma. Virchows Arch. A 422, 17-23.

Plentz R.R., André Y.N., Nellessen H., Langkopf F., Wilkens B.H.E., Ludwig M., Michael D., Fiamengo A., Roncalli B. and Rudolph M. (2007). Telomere shortening and p21 checkpoint inactivation characterize multistep hepatocarcinogenesis in humans. Hepatology 45, 968-976.

Porikli F. (2005). Integral histogram: a fast way to extract histograms in cartesian spaces. IEEE Comput. Soc. Conf. Comput. Vis. Pattern Recognit. 1, 829-836.

Rohit S. and Gaikwad M.S. (2013). Segmentation of brain tumour and its area calculation in brain MR images using K-Mean clustering and fuzzy C-Mean algorithm. Int. J. Comput. Sci. Engineering Technol. 4, 524-531.

Sakamoto M. and Hirohashi S. (1998). Natural history and prognosis of adenomatous hyperplasia to hepatocellular carcinoma: multi-institutional analysis of 53 nodules followed up for more than 6 months and 141 patients with single early hepatocellular carcinoma treated by surgical resection or percutaneous ethanol injection. Jpn. J. Clin. Oncol. 28, 604-608.

Shelhamer E., Long J. and Darrell T. (2017). Fully convolutional networks for semantic segmentation. IEEE Trans. Pattern Anal. Mach. Intell. 39, 640-651.

Shotton J., Winn J., Rother C. and Criminisi A. (2006). TextonBoost: joint appearance, shape and context modeling for multi-class object recognition and segmentation. Proc. European Conf. on Computer Vision Springer-Verlag Berlin Heidelberg. 3951, 1-15.

Stewart B. and Wild C. (2014). World cancer report 2014. Chapter 1. World Health Organization, IARC Publications.

Takayama T., Makuuchi M., Hirohashi S., Sakamoto M., Okazaki N., Takayasu K., Kosuge T., Motoo Y., Yamazaki S. and Hasegawa H. (1990). Malignant transformation of adenomatous hyperplasia to hepatocellular carcinoma. Lancet 336, 1150-1153.

Tsai A, Zhang J. and Willsky A.S. (2001). Expectation-maximization

algorithms for image processing using multiscale models and mean-field theory, with applications to laser radar profiling and segmentation. Opt. Eng. 40, 1287-1301.

Wanless I.R. (1995). Terminology of nodular hepatocellular lesions. Hepatology 22, 983-993.

Zhaomin C., Ryan B., Barrie M., Charles L.H., Heather C.A., Stephen P.P., Edward W.M., and James V.C. (2013). Infrared metrics for fixation-free liver tumor detection. J. Phys. Chem. B. 117, 12442-12450.

Zhuowen T.U., Xiangrong C., Alan L.Y, and Song-Chun Z. (2005). Image parsing: unifying segmentation, detection, and recognition. Int. J. Comput. Vis. 63, 113-140.

Accepted July 21, 2020